Mass-flowrate-maximization thermodynamic model and simulation of supersonic real-gas ejectors used in refrigeration systems

Simone Braccio, Nathan Guillou, Nicolas Tauveron, Hai Trieu Phan, Nolwenn Le Pierrès

Mass-flowrate-maximization thermodynamic model and simulation of supersonic real-gas ejectors used in refrigeration systems

Simone Braccio[1, 2, †], Nathan Guillou[1, †], Nolwenn Le Pierrès[2], Nicolas Tauveron[1], Hai Trieu Phan[1, *]

[1] *Univ. Grenoble Alpes, CEA, Liten, Campus Ines, 73375 Le Bourget du Lac, France*

[2] *LOCIE, Univ. Savoie Mont Blanc, CNRS UMR5271, Savoie Technolac, 73370 Le Bourget Du Lac, France*

[†] *These authors contributed equally to this work*

[*] *Corresponding author: Haitrieu.PHAN@cea.fr*

ARTICLE INFO

Keywords:
Supersonic ejector
Real gas
Thermodynamic modelling
Mass flow maximisation

HIGHLIGHTS

- A new thermodynamic model for ejectors based on mass flow maximization is presented
- Complex descriptions of the double-choking mechanism at play are avoided
- Model validated with R600a and R134a experimental results
- Comparative analysis on the use of different fluids is performed for a SERS cycle
- Role of the superheating and limitations for two-phase conditions are highlighted

ABSTRACT

Ejector refrigeration cycles offer an alternative to traditional systems for the production of cooling using low temperature heat. In this paper, a real gas thermodynamic model based on the mass flow rate maximisation is presented. This model has the advantage of simplifying the calculation algorithm and avoiding a complex description of the double choking mechanism taking place within the ejector. First, the model hypothesis and calculation algorithm are presented. The impact of each efficiency is evaluated and a tuning procedure is developed to calibrate the model on experimental data. Validation is performed on multiple datasets relative to two different fluids: R600a and R134a. The ejector model is then used to simulate a SERS (single ejector refrigeration system) cycle, to validate its robustness and capability to be used in the prediction of thermodynamic cycles performance. A comparative analysis of different fluids is carried out on the SERS, highlighting the important role played by the choice of the superheating. Finally, the model is used to predict performance in the case of a two-phase primary flow pointing out the limits of the model and the need of further experimental studies for the inclusion of appropriate semi-empirical corrections.

Nomenclature

A	surface	[m^2]
d	diameter	[m]
h	specific enthalpy	[$J.kg^{-1}$]
K	on-design mixing efficiency coefficient	[-]
$\dot{m}$	mass flow rate	[$kg.\ s^{-1}$]
P	pressure	[Pa]
P_c	ejector backpressure	[Pa]
$\dot{Q}$	thermal power	[kW]
s	specific entropy	[$J.\ K^{-1}.\ kg^{-1}$]
T	temperature	[K]
u	velocity	[$m.\ s^{-1}$]
$\dot{W}$	mechanical power	[kW]
x	quality	[-]

Greek letters

α	off-design mixing efficiency coefficient	[-]
η	efficiency	[-]
φ	mixing efficiency coefficient	[-]
ρ	density	[$kg.m^{-3}$]
ω	entrainment ratio	[-]

Acronyms

CFC	chlorofluorocarbon
CFD	computational fluid dynamics
COP	coefficient of performance
GWP	global warming potential
HC	hydrocarbon
HCFC	hydrochlorofluorocarbon
HFC	hydrofluorocarbon
HFO	hydrofluoroolefin
ODP	ozone depletion potential
R290	propane
R600a	isobutane
R717	ammonia
SERS	single ejector refrigeration system

Subscripts and superscripts

cri	critical point
cond	condenser
d	diffuser
evap	evaporator
gene	generator
in	inlet
is	isentropic
m	mixed flow
out	outlet
p	primary flow
s	secondary flow
pump	pump
sh	superheating
t	primary nozzle throat
y	hypothetical throat section
0	ejector inlet
1	primary nozzle inlet
1p	one-phase
2	end of mixing section
2p	two-phase
3	shock section
3	shock section
4	outlet

1 Introduction

In the current context of climate change and global warming, many new thermodynamic cycles have been developed and studied for the exploitation of low-grade heat sources (such as industrial waste heat or solar heat) to meet a growing need for refrigeration. Among the most studied low-grade heat driven refrigeration cycles, i.e. absorption cycles [1], adsorption cycles [2] and ejector cycles [3], ejector cycles are getting increasing attention.

The fundamental working principle of an ejector is to use a high-pressure flow (referred to as primary flow) to entrain and compress a low-pressure flow (referred to as secondary flow). The high-pressure primary flow enters a usually converging-diverging (though sometimes converging-only) primary nozzle inside of which it undergoes an expansion to high velocity and low pressure. The now low-pressure and high velocity primary flow is used to entrain the secondary flow from the suction chamber into the mixing chamber. In the mixing chamber, the two flows mix, and the high-speed mixed flow is decelerated in a diffuser, where it recovers pressure before leaving the ejector. The pressure of the mixed flow leaving the ejector is usually referred to as the ejector backpressure P_c. A more detailed description of the ejector working principle is presented in **Section 2**. In particular, **Fig. 1** shows a typical ejector geometry and the velocity and pressure profiles along the ejector, giving a visual representation of the thermodynamic transformations undergone by the flow during its passage in the component.

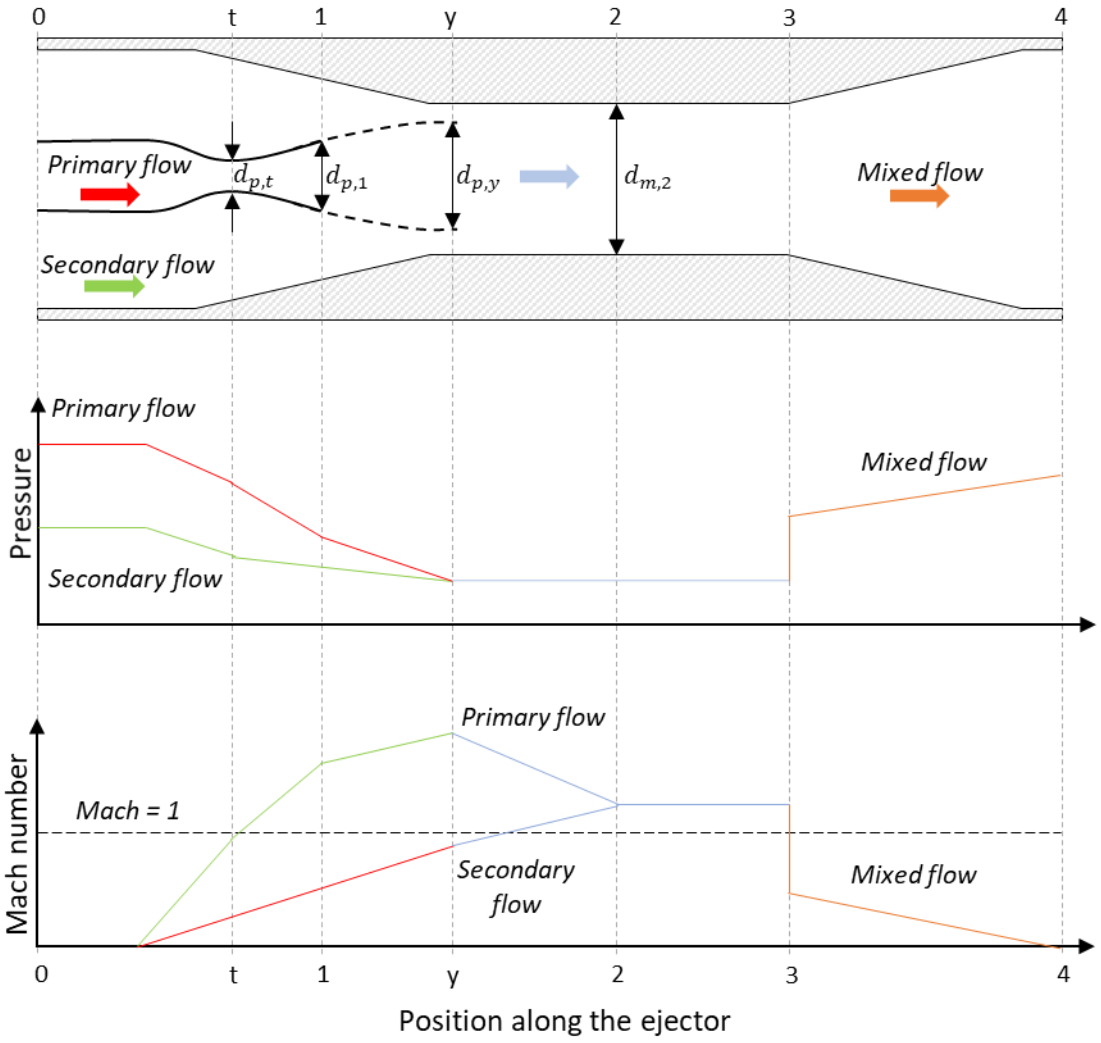

Fig. 1 - Schematic diagram of the ejector geometry and corresponding pressure and velocity profiles.

Ejectors can be used in various low-grade heat refrigeration cycles [4]. The most basic design of such cycle is the standard SERS (single ejector refrigeration system) presented on **Fig. 2**. In this cycle, the ejector is combined with three heat exchangers (condenser, evaporator and generator), a pump and an expansion valve. Low-grade heat allows the production of high-pressure primary vapour in the generator used to entrain the low-pressure secondary vapour leaving the evaporator. This cycle is the most commonly described and studied ejector cycle in literature

because of its simplicity [4]. Indeed, a large number of experimental and theoretical studies have been performed on this cycle [3][4], and their results used to improve ejector design and validate numerical models. In light of the above, the SERS is considered in this study for the validation of the developed ejector model and as a base for performance evaluation.

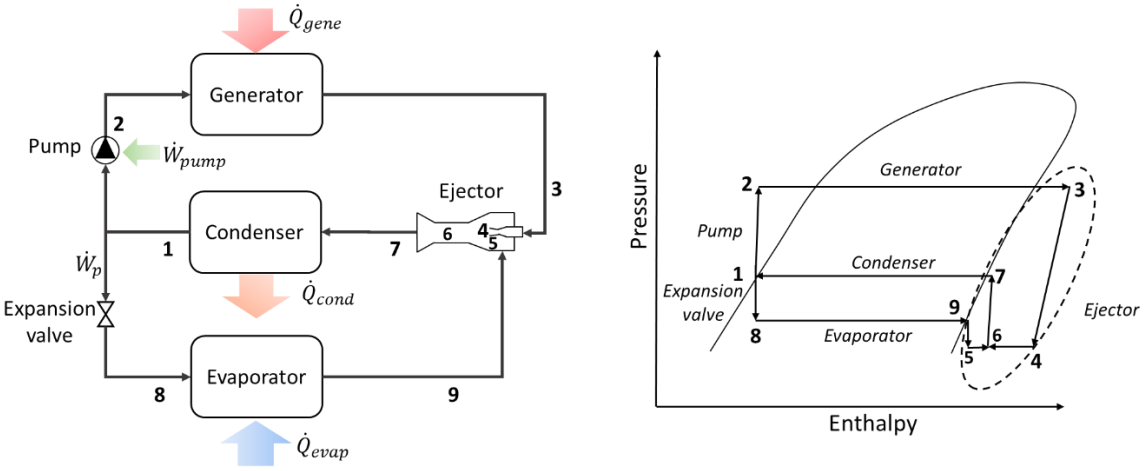

Fig. 2 - Standard ejector refrigeration cycle (SERS) schematic diagram and corresponding pressure-enthalpy diagram.

Since they have no moving parts, ejectors are very robust, reliable and are characterized by a very simple geometry involving low-maintenance and low costs. However, one of the main barriers to a widespread usage of ejector in refrigeration cycles resides precisely in their relatively narrow range of use due to the absence of control moving parts. When operating outside of their design conditions, ejectors suffer significant performance reductions and might even stop working. Thus, being able to predict ejectors performance in both on-design and off-design conditions is of paramount importance to develop thermodynamic cycles and devise appropriate control strategies. This is confirmed by the increasing number of studies that are currently being carried out with focus on the improvement of ejector models [5][6].

Different types of model are used to describe ejectors operation such as CFD models ([7][8]), zero-dimensional [9] and one-dimensional [10] empirical or semi-empirical models ([11][12]). As highlighted by He et al. [13] and Elbel et al. [3], steady-state zero-dimensional and one-dimensional models are the most studied and used type of ejector models. Indeed, the nature of flows inside ejectors being very complex (turbulent mixing, presence of shocks, condensation, two-phase flow phenomena, etc.), even more detailed models fail to precisely capture the flow patterns inside ejectors. There are two major types of steady state ejector models: single-phase (vapour) or two-phase ejector models. Single-phase ejector models are the most commonly used for refrigeration cycles, as single-phase ejectors are used in many ejector cycles, including the SERS cycle. Two-phase ejectors are used in other ejector refrigeration cycles such as transcritical ejector cycles or recirculation cycles [3]. The present model focuses on steady-state single-phase ejector thermodynamic model.

This type of model is based on the calculation of the thermodynamic state of the fluid in different sections of the ejector using mass, momentum and energy conservation equations. The first single-phase model was introduced by Keenan et al. [14] and later improved by the same authors [15]. Two types of ejectors were analysed and modelled: constant-area mixing and constant-pressure mixing ejectors. Although models for constant-area ejectors appeared to be more accurate, it was shown that constant-pressure mixing ejectors had better performance than constant-area mixing ejectors. Thus, starting from 1950, several studies focused on constant-pressure mixing ejector modelling [16][17]. Based on Keenan et al. constant-pressure mixing model [15], Munday et al. [18] introduced the idea that primary and secondary fluid do not mix directly at the exit of the primary nozzle, but rather only start mixing at a section located further in the ejector (section y in **Fig. 1**). This model first postulated the idea of a hypothetical throat, formed by the primary flow and the ejector wall, where the secondary flow reaches chocking conditions. This theory was related to previous experimental results [19] showing chocked secondary flow patterns. This double-choking regime, also referred to as Fabri-choking, constitutes the foundation of the majority of most recent ejector models. Eames et al. [20] introduced isentropic efficiency coefficients to take into account the irreversibilities due to friction losses. Huang et al. [21] included the idea of efficiency coefficients proposed by Eames et al. [20] inside the double-choking model developed by Munday et al. [18], supposing that the hypothetical throat is located inside the constant area duct. Experimental studies [22] and [23] have shown that ejectors have different working modes, depending on the inlet and outlet conditions. The most important indication

of ejector performance is the entrainment ratio ω defined as the ratio of the motor primary flow to the entrained secondary flow:

$$\omega = \frac{\dot{m}_p}{\dot{m}_s} \tag{1}$$

Results varying the ejector backpressure for fixed inlet conditions show that the entrainment ratio remains constant when increasing the backpressure until a critical backpressure P_{cri} is reached. The working mode with a constant entrainment ratio (i.e. for $P_c < P_{cri}$) is known as the on-design or critical working mode. This working mode corresponds to the presence of a double-choking as described by [21]. For $P_c > P_{cri}$ the ejector enters a working mode in which the entrainment ratio rapidly decreases when increasing the ejector backpressure. This working mode, known as the off-design or subcritical working mode, corresponds to the case in which only the primary flow is choked (also known as single-choking). Finally if the backpressure of the ejector is further increased, the ejector starts malfunctioning and reverse flow phenomena can be observed. **Fig. 3** shows a typical characteristic curve of an ejector entrainment ratio as a function of the backpressure.

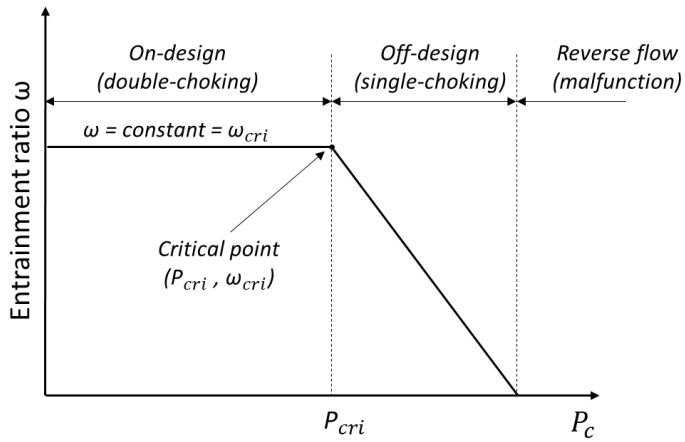

Fig. 3 - Schematic view of ejector operational modes.

The model proposed by Huang et al. [21] was able to describe the performance of the ejector in on-design working mode, but did not describe the off-design behaviour. Based on [21], Chen et al. [24] developed the first model that could predict the performance of the ejector in both on- and off-designs working mode formulating the mixing efficiency in off-design working mode as a linear function of the back pressure. This model, based on the ideal gas assumption, was later adapted by the same authors to take into account real-gas behaviour [25]. More recently, Metsue et al. [26] developed a real gas thermodynamic model, modifying the model of Chen et al. [25] to integrate the compound-choking theory, proposed by Bernstein et al. [27] and by Lamberts et al. [28] for perfect-gas ejectors. While in the Fabri-choking theory the secondary flow is assumed to reach sonic conditions in a hypothetical throat, the compound-choking theory postulates that a nozzle flow with two streams characterised by two different total pressures, can be in choking conditions with one of the streams being subsonic, if the other one is supersonic. Hence, since the combinations of two streams may behave as a sonic stream, while the Fabri-choking theory only takes into account the secondary stream, both streams are considered when analysing the choking process in the compound-choking theory [29]. This is supported by experimental [29] and numerical [30][31] studies, showing that the choking mechanism taking place does not necessarily coincides with the Fabri-choking theory since the secondary stream can remain subsonic. Metsue et al. [26] also performed an analytical study on the compound-choking criteria applied to non-isentropic perfect gas ejector showing that the use of this criterion is equivalent to maximizing the total mass flow rate within the ejector. The model presented by Metsue et al. [26] is arguably one of the most detailed steady-state thermodynamic single-phase ejector model developed to date. The compound-choking theory appears to yield more accurate results than the Fabri-chocking theory, but has however some limitations that will be further discussed in **Section 2**. The present model is based on the works Chen et al. [25] and Metsue et al [26], with the difference that mass flow-rate maximization is directly applied instead of using a specific double-choking criterion (Fabri-choking or compound choking). This avoids the use of a more complex description of the on-design double-choking phenomena and simplifies considerably the calculation algorithm. Finally, using the mass flow rate maximization eliminates the spurious overshoot around P_{cri}, described in **Section 2**, present in most other models.

2 Ejector model

This study presents an updated thermodynamic real-gas model for supersonic ejectors capable of predicting performance in both the critical and sub-critical regimes.
Metsue et al. [26] observed that both the Fabri and the compound-chocking criterion (as defined by Croquer et al. [32]) do not maximize the entrainment ratio (and thus the total mass flow rate) in the case of non isentropic flows. As explained by Croquer et al. [32], since these criteria are obtained with the hypothesis of isentropic flow, when losses are introduced through isentropic efficiencies, they are not rigorously correct and accurate anymore. Therefore, characteristic curves obtained with these models are spoiled by the presence of spurious overshoots in the near-critical off-design part of the curve, where the entrainment ratio is higher than in the on-design working mode. This behaviour, not present in experimental tests, is in contradiction with the double-choking theory, starting point of such models. Indeed, the primary definition of a choked-flow is constituted by the mass flow rate maximization and therefore, entrainment ratio and total mass flow rate cannot be higher than in the critical chocked point. It is worth mentioning that, when using such models for ejector design, the accurate prediction of the maximum mass flow rate and pressure is of paramount importance to guarantee good performance. Hence, Metsue et al. [26] proposed a corrected expression for the compound choking criteria generalised to the case of non-isentropic perfect gas flow. The authors showed that the application of this criterion is equivalent to mass flow rate maximization of the flow within the ejector, thus proving the choking mechanism at play in supersonic ejectors is indeed the compound-choking. Since the two criteria lead to the same results it is possible to use mass flow rate maximization when dealing with non-isentropic flows. Metsue et al. [26] solved the primary flow by maximizing the mass flow rate instead of imposing Mach equal to unity, but did not present a calculation procedure for the maximization of the total mass flow rate. Instead, the algorithm presented used the compound choking theory [26]. In the present work, both the primary flow and the total ejector mass flow rate are found by imposing the maximization of mass flow rate. To do so, the off-design mass flow rate characteristic of the ejector is calculated and its maximum taken as the critical mass flow rate. The aim of this approach is to simplify the calculation algorithm and to avoid a complex description of the double-choking mechanism at play. The validation of this model on experimental results available in literature, shows its capability to predict very accurately the critical conditions of the ejector (P_{cri}, ω_{cri}). This makes the model a very valuable tool, not only for simulation of thermodynamic cycles, but also for ejector preliminary design.

2.1 Model hypothesis

The ejector geometry used in this study is presented on **Fig. 1.** It is the constant pressure geometry considered by Munday et al. [18] and Huang et al. [21]. The presented schematization of the flows within the ejector is the one based on the double-choking theory. The primary flow enters the converging part of the primary nozzle at section *0* and is expanded and accelerated up to the primary nozzle exit. The secondary flow enters the suction chamber at section *0* and is entrained by the primary flow inside the mixing section. The primary flow continues its expansion outside the primary nozzle, forming a converging duct for the secondary flow. Consequently, the secondary flow is also separately accelerated and expanded up to section *y*. As supposed by Munday et al. [18], the assumption is also made that the two flows do not start mixing until section y, located in the constant area mixing section. The flows mix at constant pressure and are assumed to be fully mixed at section 2. The mixed fluid usually undergoes a normal shock at section 3 up to reaching subsonic velocities. A subsonic diffusion takes place in the diffuser where the flow is slowed down and pressure is recovered. The velocity and pressure profiles resulting from these hypotheses are shown in **Fig. 1.** The model is based on mass, momentum and energy balance equations between the different sections. Additionally, the following assumptions are made:

- The flows are steady and one-dimensional
- Adiabatic flow
- Kinetic energy at primary nozzle inlet, suction chamber inlet and diffuser outlet is negligible
- Non-isentropic phenomena are taken into account through isentropic and mixing efficiencies η_p, η_{py}, η_s, η_m and η_d (setting of these efficiencies will be further discussed in **Section 3**)

Partial condensation or flashing can take place inside the ejector [33]. When this is the case, the homogeneous equilibrium hypothesis is used in the present model. As explained in [34], this assumption allows treating the flow within the ejector as steady-state and one-dimensional even when the fluid becomes a liquid-vapour two-phase mixture.

The model was developed in EES® (Engineering Equation Solver) [35] using EES® internal thermodynamic libraries for the different fluids. The model can be used both to simulate ejector performance and for the preliminary design of the ejectors characteristics sections, as explained in **Section 4**.

2.2 Computational procedure

Fig. 4 shows the calculation algorithm developed for the present model. The inputs are:

- The ejector geometry and in particular the primary nozzle throat diameter $d_{p,t}$, primary nozzle exit diameter $d_{p,1}$, and mixing chamber diameter $d_{m,2}$
- The isentropic efficiencies η_p, η_{py}, η_s and η_d as well as the two coefficient φ_m and α_m that define the mixing efficiency η_m as detailed in **Section 2.5.**
- The inlet and outlet conditions of the ejector: pressure and enthalpy at the primary nozzle entrance ($P_{p,0}$ and $h_{p,0}$), at the suction chamber entrance ($P_{s,0}$ and $h_{s,0}$), and the ejector backpressure P_c.

Clearly, the thermodynamic state of the flows entering the ejector is then fully determined and in particular the entropies $s_{s,0}$ and $s_{p,0}$ are also known:

$$s_{p,0} = s(P_{p,0}, h_{p,0}) \quad (2)$$

$$s_{s,0} = s(P_{s,0}, h_{s,0}) \quad (3)$$

The outputs are the primary and secondary mass flow rates $\dot{m}_p$, $\dot{m}_s$ (and consequently the entrainment ratio of the ejector ω) and the thermodynamic state of the flow exiting the ejector.

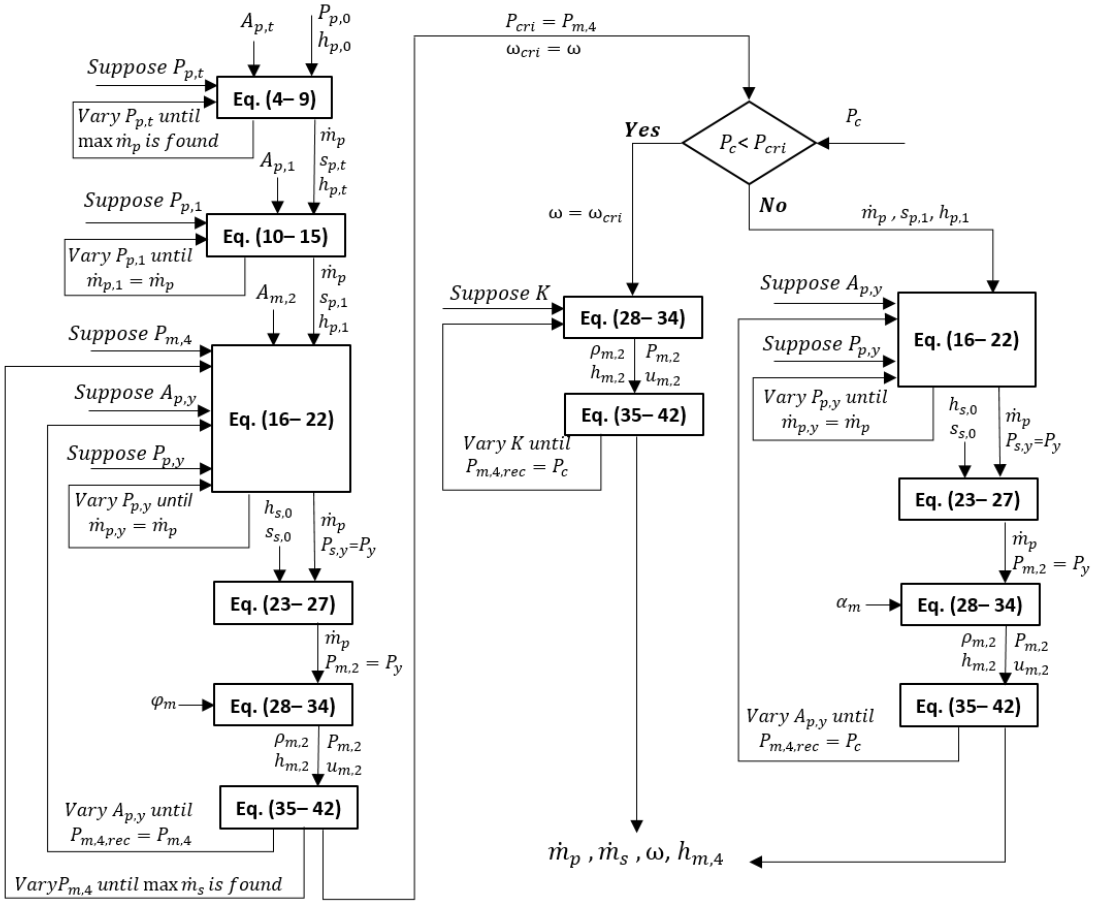

Fig. 4 - Flowchart of the performance simulation calculation procedure.

The first step of the algorithm consists in applying the maximization of mass flow rate to determine the primary mass flow rate and the properties of the fluid leaving the primary nozzle (**Section 2.3**). The second step of the algorithm consists in maximizing the ejector total mass flow rate and entrainment ratio to determine the critical point of the ejector (P_{cri}, ω_{cri}) (**Section 2.4**). Finally, once the critical point is determined, performance simulation can be carried out. To this end, equations describing the on-design or off-design working mode are used, depending on whether the actual ejector backpressure P_c is higher or lower than the critical backpressure P_{cri} (**Section 2.5**).

2.3 Primary nozzle

Choking of the primary fluid is assumed to solve the primary flow. As shown in [36], even a very small pressure difference between inlet and outlet of a converging-diverging nozzle is sufficient to achieve sonic conditions in the throat. Since pressure ratios normally encountered in ejector refrigeration cycles are generally higher, the primary nozzle nearly always works in choking conditions. This is usually imposed by setting the Mach number equal to one at the throat section [25]. However, another approach consists in maximizing the treated mass flow rate [26]. This approach was used in the present model as it yields more precise results in the case of non-isentropic expansion and does not require the computation of the sound speed.

A guess value for the pressure at the primary nozzle throat $P_{p,t}$ is supposed and updated iterating on **Eq. (4)-(8)** until a maximum for the primary flow mass flow rate $\dot{m}_p$ is found:

$$h_{p,t,is} = h(P_{p,t}, s_{p,0}) \tag{4}$$
$$h_{p,t} = h_{p,0} - \eta_p \cdot (h_{p,0} - h_{p,t,is}) \tag{5}$$
$$\rho_{p,t} = \rho(P_{p,t}, h_{p,t}) \tag{6}$$
$$u_{p,t} = \sqrt{2 \cdot (h_{p,0} - h_{p,t})} \tag{7}$$
$$\dot{m}_p = \rho_{p,t} \cdot u_{p,t} \cdot A_{p,t} \tag{8}$$

The entropy of the fluid at the primary nozzle throat is then also determined:

$$s_{p,t} = s(P_{p,t}, h_{p,t}) \tag{9}$$

Similarly, also for the diverging part of the nozzle an exit pressure value $P_{p,1}$ is supposed and **Eq. (10)-(14)** are solved iteratively, changing $P_{p,1}$ until the exit mass flow rate equals the one calculated for the nozzle throat:

$$h_{p,1,is} = h(P_{p,1}, s_{p,t}) \tag{10}$$
$$h_{p,1} = h_{p,t} - \eta_p \cdot (h_{p,t} - h_{p,1,is}) \tag{11}$$
$$\rho_{p,1} = \rho(P_{p,1}, h_{p,1}) \tag{12}$$
$$u_{p,1} = \sqrt{2 \cdot (h_{p,t} - h_{p,1}) + {u_{p,t}}^2} \tag{13}$$
$$\dot{m}_p = \rho_{p,1} \cdot u_{p,1} \cdot A_{p,1} \tag{14}$$

The state of the fluid leaving the primary nozzle is then fully determined and, in particular, the value of the entropy is:

$$s_{p,1} = s(P_{p,1}, h_{p,1}) \tag{15}$$

2.4 Critical point determination through entrainment ratio maximization

Once the flow in the primary injector is solved, the critical point determination can be performed though the entrainment ratio maximization (i.e. the maximization of the secondary flow mass flow rate, since the primary flow mass flow rate was already determined in the previous step), necessary before performance simulation.
For a given ejector backpressure $P_{m,4}$, **Eq. (16)-(42)** are used to compute the secondary mass flow rate $\dot{m}_s$ and therefore the value of the entrainment ratio corresponding to the backpressure $P_{m,4}$. The indication $P_{m,4}$ is used here for a generic backpressure on which an iterative process is performed for the critical point determination. This is done to distinguish $P_{m,4}$ from the actual ejector backpressure P_c used for performance simulation in **Section 2.5**.

As previously explained, it is assumed that the primary and secondary flow start a constant pressure mixing process at section y in the constant area section of the ejector. Therefore, by initially taking a guess value for $A_{p,y}$, it is possible to write:

$$A_{s,y} = A_{m,2} - A_{p,y} \tag{16}$$

$$P_{s,y} = P_{p,y} \tag{17}$$

The same equations used before are applied between the primary nozzle exit and section y to find the pressure $P_{p,y}$ allowing the conservation of the primary fluid mass flow rate. The only difference with respect to before is that in this case **Eq. (19)** also takes into account the possibility of a recompression taking place from section 1 to section y [36]:

$$h_{p,y,is} = h(P_{p,y}, s_{p,1}) \tag{18}$$

$$h_{p,y} = h_{p,1} - \max\left[\eta_{py} \cdot \left(h_{p,1} - h_{p,y,is}\right), 0\right] + \max\left[\frac{(h_{p,y,is} - h_{p,1})}{\eta_{py}}, 0\right] \tag{19}$$

$$u_{p,y} = \sqrt{2 \cdot (h_{p,1} - h_{p,y}) + {u_{p,1}}^2} \tag{20}$$

$$\rho_{p,y} = \rho(P_{p,y}, h_{p,y}) \tag{21}$$

$$\dot{m}_p = \rho_{p,y} \cdot u_{p,y} \cdot A_{p,y} \tag{22}$$

Similarly, **Eq. (23)-(27)** describe the expansion of the secondary fluid between the suction chamber inlet and the beginning of mixing sections:

$$h_{s,y,is} = h(P_{s,y}, s_{s,0}) \tag{23}$$

$$h_{s,y} = h_{s,0} - \eta_s \cdot (h_{s,0} - h_{s,y,is}) \tag{24}$$

$$u_{s,y} = \sqrt{2 \cdot (h_{s,0} - h_{s,y})} \tag{25}$$

$$\rho_{s,y} = \rho(P_{s,y}, h_{s,y}) \tag{26}$$

$$\dot{m}_s = \rho_{s,y} \cdot u_{s,y} \cdot A_{s,y} \tag{27}$$

Eq. (28)-(34) describe the mixing process that occurs between sections y and 2. The mixing efficiency η_m is used to take into account the irreversibilities of the mixing process and is initially considered equal to the input parameter φ_m :

$$\dot{m}_m = \dot{m}_p + \dot{m}_s \tag{28}$$

$$P_{m,2} = P_{p,y} \tag{29}$$

$$u_{m,2,is} = \frac{\dot{m}_p \cdot u_{p,y} + \dot{m}_s \cdot u_{s,y}}{\dot{m}_m} \tag{30}$$

$$\eta_m = \varphi_m \tag{31}$$

$$u_{m,2} = \sqrt{\eta_m} \cdot u_{m,2,is} \tag{32}$$

$$h_{m,2} = \frac{\dot{m}_p}{\dot{m}_m} \cdot \left(h_{p,y} + \frac{{u_{p,y}}^2}{2}\right) + \frac{\dot{m}_s}{\dot{m}_m} \cdot \left(h_{s,y} + \frac{{u_{s,y}}^2}{2}\right) - \frac{{u_{m,2}}^2}{2} \tag{33}$$

$$\rho_{m,2} = \rho(P_{m,2}, h_{m,2}) \tag{34}$$

The mixed fluid at section 2 is usually (although not necessarily [26]) still supersonic, but the fluid leaving the ejector is subsonic therefore a diffusion must take place. This recompression can only be brought about by a shock wave because a convergent duct is necessary for isentropic diffusion of a supersonic stream [37][38]. For simplicity, it is assumed that a normal shock occurs in the constant section area after the end of the mixing process, before entering the diffuser. The Rankine-Hugoniot equations that govern this shock are:

$$\rho_{m,3} = \rho(P_{m,3}, h_{m,3}) \tag{35}$$

$$u_{m,3} = \frac{\rho_{m,2} \cdot u_{m,2}}{\rho_{m,3}} \tag{36}$$

$$h_{m,3} = h_{m,2} + \frac{{u_{m,2}}^2}{2} - \frac{{u_{m,3}}^2}{2} \tag{37}$$

$$P_{m,3} = \rho_{m,2} \cdot {u_{m,2}}^2 + P_{m,2} - \rho_{m,3} \cdot {u_{m,3}}^2 \tag{38}$$

When the flow is supersonic, in addition to the trivial solution in which all quantities remain the same, this set of equations has another solution, relative to the presence of a shock, which can be found by setting appropriately different guess values [37][38]. The entropy after the shock is:

$$s_{m,3} = s(P_{m,3}, h_{m,3}) \tag{39}$$

Finally, the mixed fluid undergoes a compression in the diffuser before leaving the ejector:

$$h_{m,4} = h_{m,3} + \frac{{u_{m,3}}^2}{2} \tag{40}$$

$$h_{m,4,is} = h_{m,3} + \eta_d \cdot (h_{m,4} - h_{m,3}) \tag{41}$$

$$P_{m,4,rec} = P(h_{m,4,is}, s_{m,3}) \tag{42}$$

For a given value of $A_{p,y}$, mixing, normal shock and diffusion equations allow the unambiguous determination of the exit pressure $P_{m,4,rec}$ which however may not coincide with the input $P_{m,4}$.
Indeed, while $A_{m,2}$ is an input parameter relative to the geometry of the ejector, the hypothetical section $A_{p,y}$ used in **Eq. (16)** is not known from the beginning. A guess value is therefore needed and an iterative calculation has to be performed until the recalculated $P_{m,4,rec}$ equals the input generic input pressure $P_{m,4}$. In order to determine the critical working point of the ejector the maximization of the total mass flow rate is used. This is done by changing the value of the backpressure $P_{m,4}$ and updating **Eq. (16)-(42)** until the value of P_{cri} corresponding to the maximum entrainment ratio ω_{cri} is found. It is worth mentioning that, since in this study the model is developed in EES®, all the iterative process described above do not need to be carried out explicitly. In fact, in view of the fact that EES® is an equation solver, it is sufficient to input the right number of equations and constraints and the software will perform the iterative processes internally

2.5 Performance simulation

After the critical point (P_{cri} and ω_{cri}) is determined, simulation of the ejector performance can be carried out. Performance simulations is executed using essentially the same equations needed for the performance critical point determination. Some differences are however introduced depending on whether the ejector is functioning in the on-design or in the off-design working mode.

On-design working mode

If the actual backpressure of the ejector is lower than the critical backpressure (i.e : $P_c < P_{cri}$), the ejector is in on-design working mode with a choking of both the primary and secondary flow. The equations describing the transformations undergone by the fluid are the same as in **Section 2.4** with a few differences:

- $P_{m,4}$ is replaced by the actual backpressure value P_c
- The entrainment ratio is imposed to be equal to the critical entrainment ratio ($\omega = \omega_{cri}$)
- A coefficient K is added to the definition of the mixing efficiency of **Eq. (31)**:

$$\eta_m = K \cdot \varphi_m \tag{43}$$

Note that this approach is possible because the critical point (P_{cri}, ω_{cri}) is determined beforehand. Since the entrainment ration is imposed equal to the previously determined ω_{cri}, the coefficient K is used to give one needed degree of freedom to the set of equations. This coefficient considers the adjustment loss phenomena enabling the ejector to reach the imposed backpressure in the on-design working mode.

Off-design working mode

If the actual backpressure of the ejector is greater than the critical backpressure (i.e. : $P_c > P_{cri}$), the ejector works in off-design working mode, where only the primary flow is choked. Also, in this case the necessary equations remain largely unchanged from those described in **Section 2.4** with the only differences that:

- $P_{m,4}$ is replaced by the actual backpressure value P_c.
- The expression for the mixing efficiency becomes:

$$\eta_m = \varphi_m \cdot \left[1 - \alpha_m \cdot \left(\frac{P_c - P_{cri}}{P_c}\right)\right] \tag{44}$$

Eq. (44) describes the off-design efficiency of the mixing process. φ_m and α_m are input parameters that are tuned on experimental data (see **Section 3**). The linear dependency of the mixing efficiency from the back-pressure in off-design mode, first implemented by Chen et al. [25], results in a better fit with experimental data.

3 Model validation and coefficients calibration

3.1 Parameters tuning

Experimental datasets are used to validate the model and its ability to accurately describe ejectors performance. As explained in **Section 2**, irreversibilities occurring inside the ejector are considered in the model through efficiency coefficients. The typical approach when comparing thermodynamic models and experimental results consists in tuning efficiency coefficients for each fluid in order to obtain the best possible match with experimental results. However, experimental data are needed for each fluid studied and the tuning process must be repeated. The impact of each of the ejector efficiency coefficient has been investigated in various studies ([39][40][41] [26]). **Fig. 5**, in accordance with existing literature, shows the influence of η_p, η_s , φ_m and α_m values on the primary and secondary mass flow rates. **Fig. 5** was obtained through the simulation of the SERS cycle of **Fig. 2**, using R290 as refrigerant. The primary and secondary mass flow rate are plotted versus the ejector backpressure. Four parameters are considered to evaluate the impact of each efficiency: the value of the primary mass flow rate, the value of the on-design secondary mass flow rate, the value of the critical backpressure and the slope of the off-design secondary mass flow rate curve.

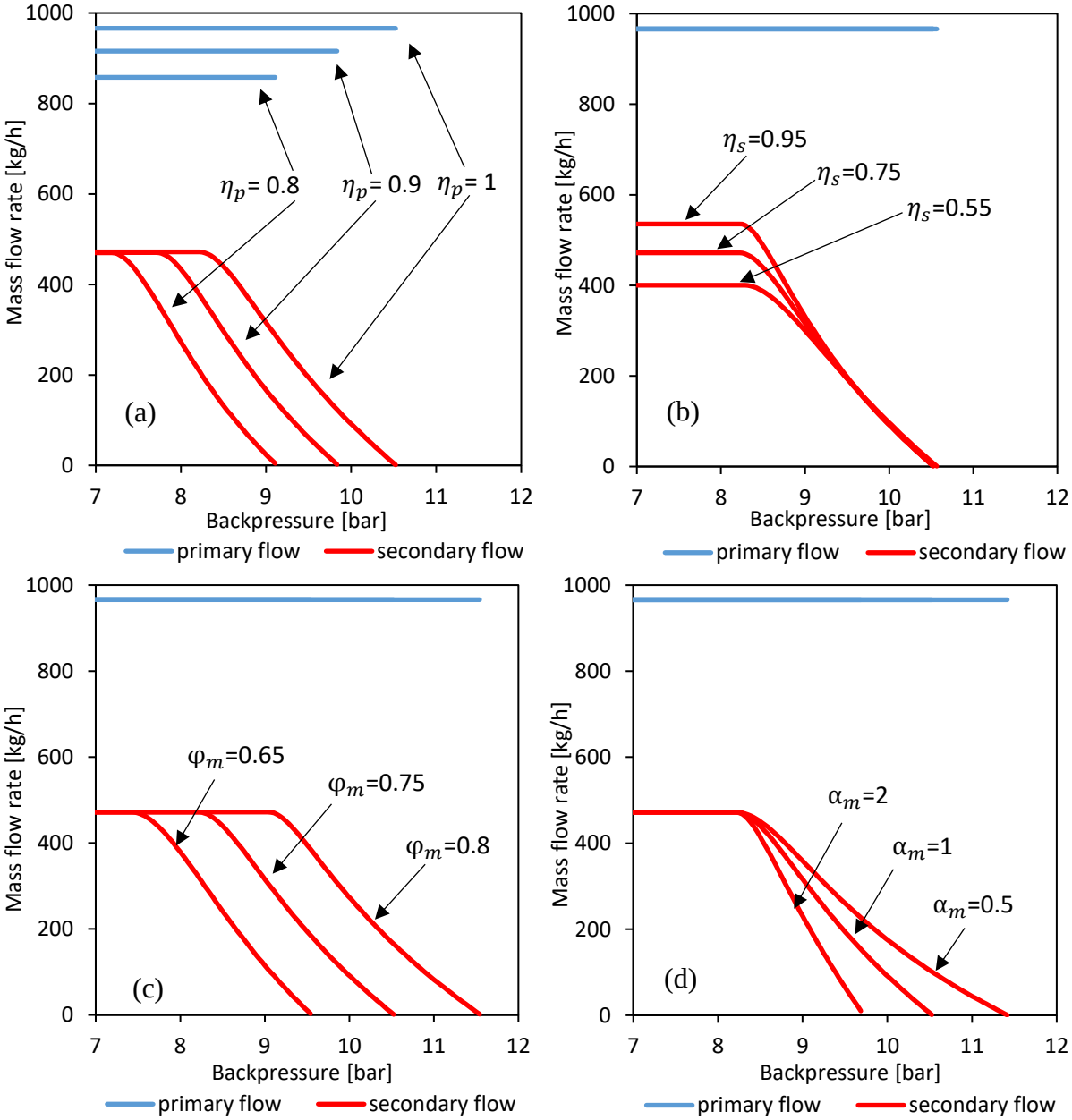

Fig. 5 - Impact of the efficiency coefficients on the primary and secondary mass flows variations as a function of the ejector backpressure.

The nozzle efficiency η_p (**Fig. 5 (a)**) only affects the primary mass flow rate and the value of P_{cri}. An increase of η_s (**Fig. 5 (b)**) leads to a higher on-design secondary mass flow rate with no impact on other quantities. A variation of φ_m **Fig. 5 (c)** is instead directly linked to a variation of the critical backpressure. Finally, α_m (**Fig. 5 (d)**) determines the slope of the off-design curve. The impact of η_{py} and η_d was also studied, validating the observations of [26]: a variation of η_{py} has the same effect as a variation of η_s, while changing η_d is equivalent to changing φ_m. Therefore, here it was chosen to only tune η_p, η_s , φ_m and α_m to fit experimental results while η_{py} and η_d were fixed to 0.99, assuming surface conditions guaranteeing an almost isentropic flow.

Considering that each efficiency has a different impact on the performance of the ejector, the following fitting procedure was applied:

- η_p is adjusted to match the experimental and primary fluid mass flow rates. Unfortunately, in most of experimental studies available in the literature the primary mass flow rate is not given. In such cases η_p is taken equal to 0.99. This is consistent with most previous studies, where the primary nozzle efficiency is most often fixed at values between 0.95 and 1 ([15][34][42]).
- η_s and φ_m are tuned to match respectively ω_{cri} and P_{cri} thus guaranteeing a good prediction of the critical point.
- α_m is varied to approximate the experimental slope of the ejector characteristic off-design part.

When multiple datasets are available, the procedure presented above for adjusting the four coefficients η_p, η_s, φ_m and α_m is performed for each dataset and an average value is then taken for the fluid considered.
Two examples of model validation/experimental data fitting through the adjustment of those coefficients are presented in **Section 3.2** and **Section 3.3**.

3.2 Calibration of an R600a ejector

The validation of the model for the case of R600a (isobutane) was performed using data from Butrymowicz et al. [43] referring to a solar-powered SERS using R600a . The dimensions of the ejector studied are: $d_{p,t}$= 3.5mm, $d_{p,1}$= 5mm and $d_{m,2}$= 6mm. Four datasets are present in the study referring to the variation of the condensation temperature for different generator temperature (55-63.5°C) but constant evaporator temperature (7°C), superheating at evaporator outlet (6.5°C), and superheating at generator outlet (8°C).

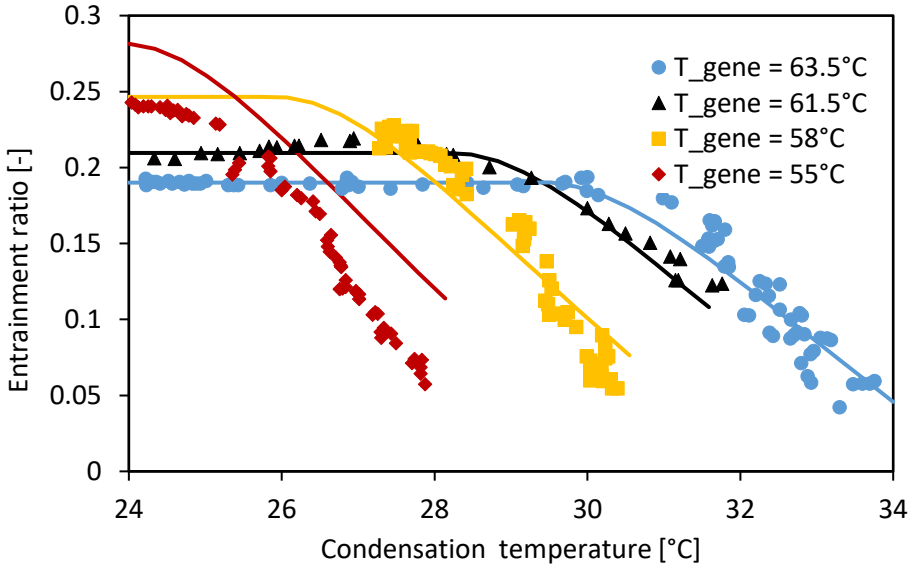

Fig. 6 - Simulation model results (lines) compared to the experimental results (markers) from [43]: impact of the condensation temperature on the entrainment ratio, for different generator temperatures.

In this study, no precise information on the primary mass flow was available so η_p was set to 0.99. The adjusted efficiency coefficients that give the best fitting between experimental theoretical data are found to be η_s= 0.77, φ_m= 0.72 and α_m= 0.99. **Fig. 6** shows the results of the model using the adjusted coefficient (lines) compared to

the experimental results (markers). It can be noted that, for the two highest generator temperatures (T_{gene}= 61.5°C and T_{gene}= 63.5°C) the ejector operates in both on-design and off-design modes, the on-design mode being easily recognizable by the constant entrainment ratio plateau. For the two other experimental datasets (T_{gene}= 58°C and T_{gene}= 55°C), only off-design conditions are present. The numerical model predicts very well the on-design plateau and the location of the critical point. The model also appears to fit quite well the off-design operation of the ejector, except for the case of T_{evap}= 55°C where the model seems to overestimate the entrainment ratio.

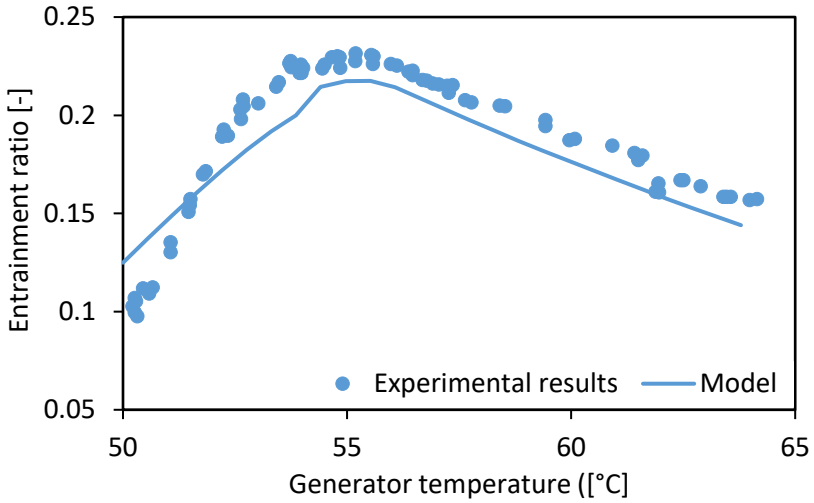

Fig. 7 - Simulation model results (lines) compared to the experimental results (markers) from **[43]**: impact of the generator temperature on the entrainment ratio.

Fig. 7 compares the results of the model and experimental results at the variation of the generator temperature while keeping all other parameters constant (condenser temperature 24 °C and evaporator temperature 3.5 °C). Experimental tendencies are respected, especially in the on-design working mode (T_{gene}>55°C), and position of the critical point is accurately predicted.

3.3 Calibration of an R134a ejector

A second fitting procedure was performed for R134a using experimental data from Hakkaki-Fard et al. [44] where three different ejector geometries are studied (referred to as EJEI, EJEII and EJEIII). Inlet conditions in the study are specifically fixed for each ejector geometry while the backpressure is varied.

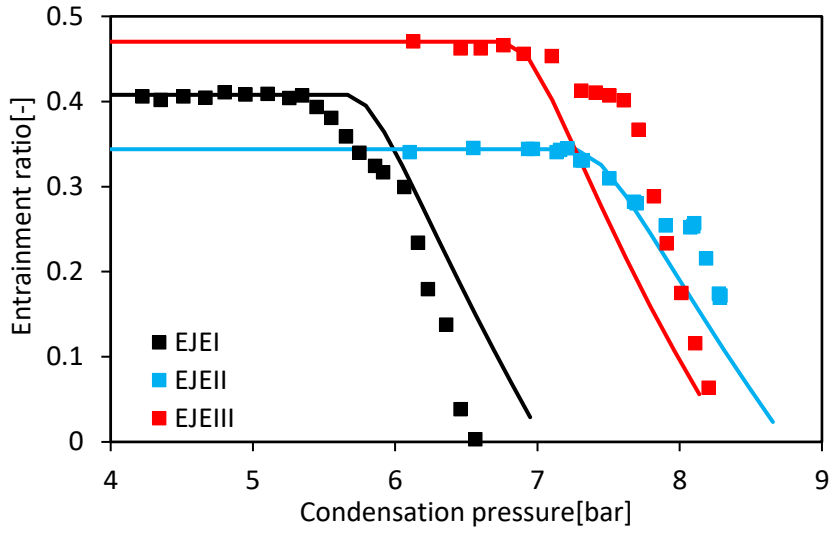

Fig. 8 - Simulation model results compared to the experimental results from [44] for the effect of the condensation pressure on the entrainment ratio, for different ejector geometries and inlet conditions.

Since also in this case no information is available concerning the primary fluid mass flow rate, η_p was fixed at 0.99. The adjusted coefficient guaranteeing the best accordance with experimental results are found to be: η_s=0.72, φ_m=0.76 and α_m=1.46.
Fig. 8 shows the adjusted model output (lines) compared to experimental results (markers). Each of the three datasets in the picture refers to one particular ejector geometry operating at its specific working conditions. For the three different geometries, the model fits well the experimental data (**Fig. 8),** predicting accurately the on-design plateau and the location of the critical point. The off-design part of the ejector characteristic is also well approximated.

The same experimental Hakkaki-Fard et al. [44] results and results from the present model shown in **Fig. 8** are divided into 3 subplots (one for each ejector geometry) in **Fig. 9** and compared to CFD results from [44] and to 1D thermodynamic model based on the compound choking theory from [26]. Compared to the CFD model, the present model is able to give an equally accurate prediction of the on-design operation and critical point location but appears to be less accurate in the description of the off-design behaviour of the ejectors. Compared to the thermodynamic model based on the compound choking theory from [26], the present model yields more accurate results in the on-design functioning mode, while results in the off-design functioning mode are comparable.

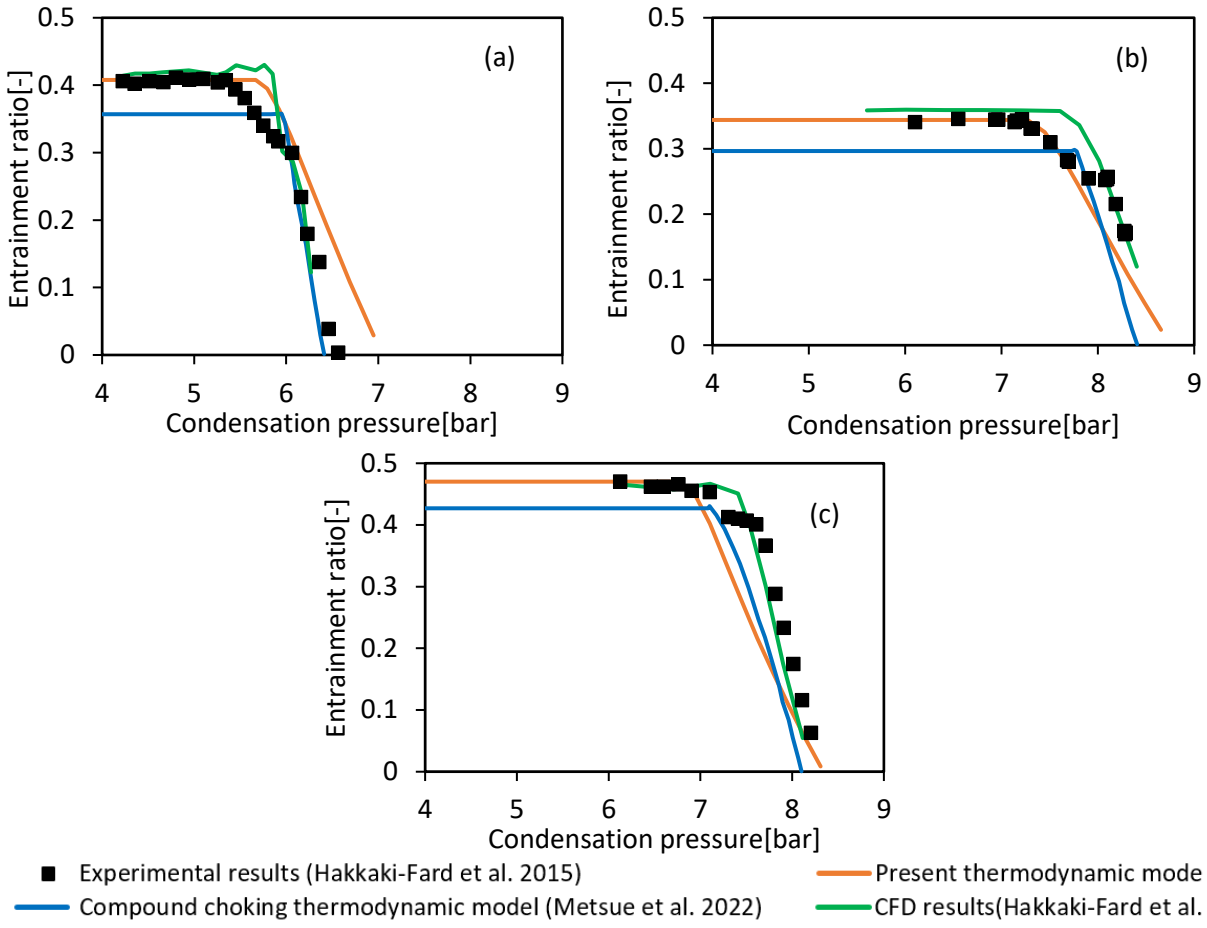

Fig. 9 - Simulation model results (lines) compared to the experimental results (markers) from [44], CFD results from [44], and results from compound choking 1D model [26], for the effect of the condensation pressure on the entrainment ratio, for three different ejector geometries and inlet conditions ((a): EJEI, (b): EJEII and (c): EJEIII).

4 Case study: design of an ejector for a SERS cycle

4.1 Context and fluid selection

4.1.1 Context of the case study

The present model was used to simulate a SERS cycle (**Fig. 2)** to prove its robustness and ability to be used in the performance evaluation of thermodynamic cycles and for ejector preliminary design. In the application considered, the evaporator temperature is taken constant and equal to 5°C, the condenser temperature is taken equal to 20°C while the generator temperature is varied between 60°C and 150°C. The available thermal power at the generator is supposed equal to 100 kW. Seven different working fluids are tested and their performance compared. For each fluid, the ejector model is used to find the optimal ejector geometry for each working condition considered. Performance of the SERS cycle integrating optimal geometry ejectors is then compared for the different fluids to give some insights on the choice of the most appropriate fluid. The performance of the cycle is measured by its COP, defined as the cooling power output produced at the evaporator over the sum of the thermal power input at the generator and the pump work:

$$COP = \frac{\dot{Q}_{evap}}{\dot{Q}_{gene} + \dot{W}_{pump}} \tag{45}$$

The pump was modelled using a fix isentropic efficiency of 0.9 [45], although the pumping work is usually very small with respect to thermal powers in **Eq. (45)**. If the pumping work is neglected, the COP of the cycle can be written as [46]:

.

$$COP = \frac{\dot{m}_s \cdot (h_{evap,out} - h_{evap,in})}{\dot{m}_s \cdot (h_{gene,out} - h_{gene,in})} = \omega \cdot \frac{h_{evap,out} - h_{evap,in}}{h_{gene,out} - h_{gene,in}} \tag{46}$$

in which the use of **Eq.(1)** highlights how the system efficiency is directly affected by the ejector performance.

4.1.2 Selection of the study fluids

In the current context of climate change and global warming, an increasing attention is drawn to the refrigerant fluid selection. The identification of environmentally friendly fluids as an alternative to the currently used refrigerants represents today a major challenge [47]. Montreal Protocol (1987), Kyoto Protocol (1997), Paris agreement (2015) and Kigali amendment (2016) have forced the phase-down of CFCs, HCFCs and more recently of most HFCs. EU's F-gas regulation (EU regulation n° 517/2014) imposes GWP limits for the fluids used in different applications. In particular, a maximum GWP of 150 is applied to many domestic, commercial and industrial refrigeration and air-conditioning systems. R134a, currently the most used fluid in these systems, has a GWP of 1300 and suitable replacements need to be found.
Possible replacements of R134a for such systems include:

- Natural fluids: HCs (hydrocarbons) such as R290 (propane), R600a (isobutane) and R1270 (propylene) and inorganic refrigerants such as CO_2 (carbon-dioxide) and R717 (ammonia).
- HFOs (hydro-fluoro-elements) that are unsaturated HFCs, such as R1234yf and R1234ze(Z).
- Blends like HFC/HC blends, HC/HC blends or HFC/HFO blends.

Table 1 - Main properties of the fluids selected for the study.

	R134a	R152a	R290	R600a	R717	R1234yf	R1234ze(Z)
Fluid type	Wet	Wet	Wet	Dry	Wet	Isentropic	Isentropic
Fluid class	HFC	HFC	HC	HC	-	HFO	HFO
Critical Temperature [°C]	101.1	113.3	96.7	134.7	132.4	94.7	150.1
Critical Pressure [bar]	40.6	45.2	42.5	36.3	113.6	33.8	35.3
ODP	0	0	0	0	0	0	0
GWP	1430	124	20	20	<1	4	7
ASHRAE safety class	A1	A2	A3	A3	B2L	A2L	A2L

In light of the above, seven fluids are considered in the application of the ejector model to the SERS cycle, as shown in **Table 1**. In particular they are two HFCs (R134a and R152a), two HFOs (R1234yf and R1234ze(Z)), two hydro-carbons (R290 and R600a) and an inorganic natural refrigerant (R717). R134a is considered as reference for performance comparison. R152a is also used in the study, as it is an HFC with a GWP lower than the 150 actual limit. Finally, the five other fluids represent the most commonly studied environmentally friendly replacements to R134a.

4.2 Ejector design

4.2.1 Design model

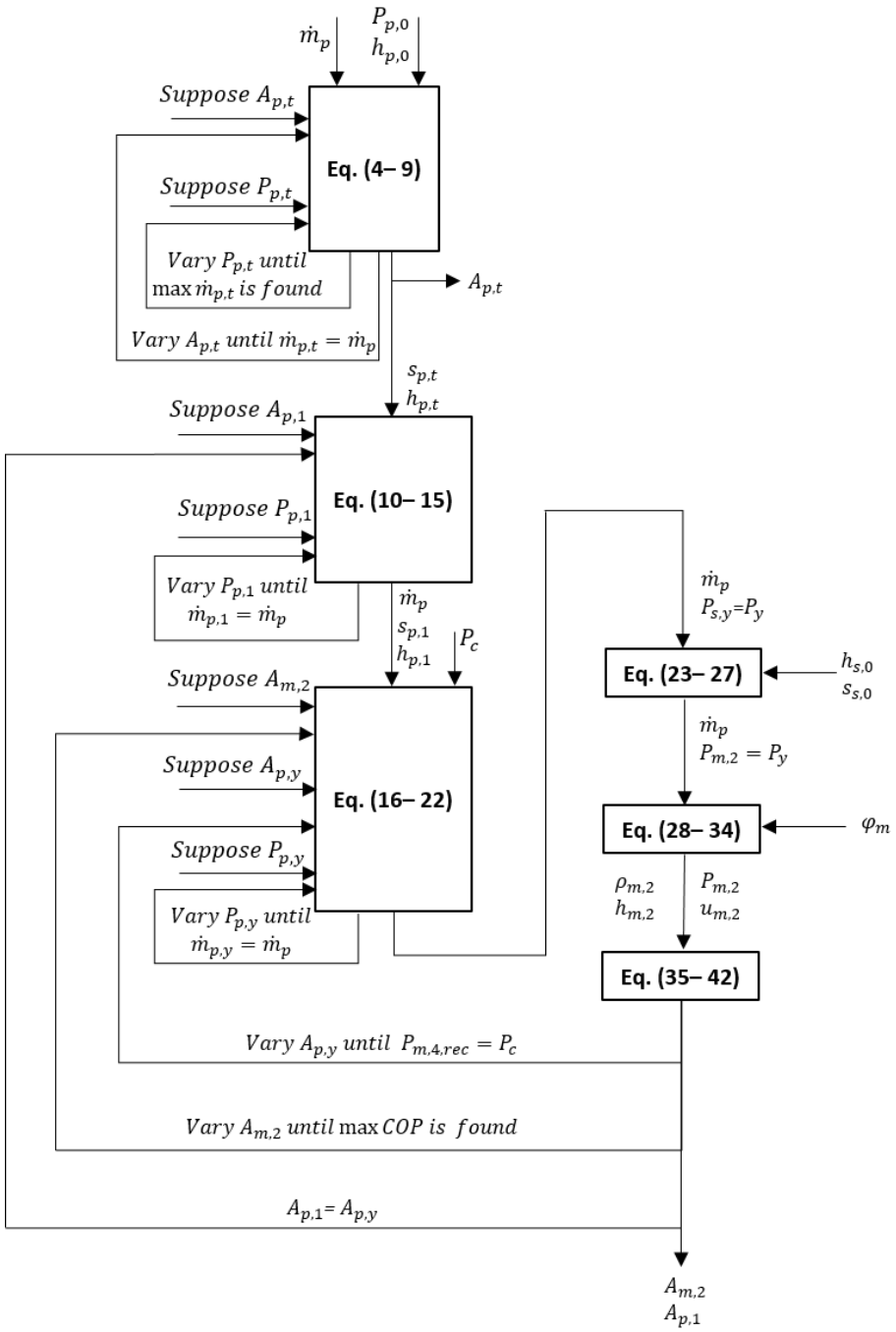

Fig. 10 - Flowchart of the design procedure.

Fig. 10 shows the calculation algorithm to be used in the case of design. The geometry of the ejector (i.e. primary nozzle throat and exit diameter $d_{p,t}$, and $d_{p,1}$, and mixing chamber diameter $d_{m,2}$) is in this case an output of the model. Mass flow rate and inlet conditions of the fluid being fixed by the available heat source and the chosen superheating of the vapour, the primary nozzle throat section (i.e. $d_{p,t}$) is easily accessible through **Eq. (8)**. The choice of the superheating is a very influential parameter on the performance of the cycle and will be further discussed in **Section 4.2.3**. Furthermore, the diameter of the mixing chamber $d_{m,2}$ is obtained by maximizing the COP of the cycle. Finally, it is worth mentioning that the impact of $d_{p,1}$ on the entrainment ratio of the ejector (and thus on the COP of the cycle) is not very important in this model. This is because the primary nozzle is virtually extended up to the hypothetical throat section whose position has in turn a very important impact on the component performance. In the study, the primary nozzle exit diameter is set through **Eq. (47)**, so that the flow leaving the primary nozzle is in adapted conditions, with no compression or further expansion taking place outside the nozzle (thus avoiding further irreversibilities).

$$A_{p,1} = A_{p,y} \tag{47}$$

4.2.2 Application to the studied fluids

Even though it was shown in **Section 3** that efficiency coefficients should be calibrated for each fluid, experimental data were not available for all of the seven fluids selected for the comparative study so the ejector efficiency coefficients calibration was not possible for all of the seven fluids tested. For this reason, the same ejector efficiencies were considered for all the fluids, and particularly average values with respected to the two calibrations were used: $\eta_p = 0.99$, $\eta_s = 0.75$, α_m= 1.23 , which are close to the values found during the calibrations of **Section 3**. Note that since ejectors are designed to work at their critical-point the value of φ_m is not very important since it does not intervene in the critical point determination and has only an impact in the off-design functioning. Using the same efficiencies for all the different fluids and geometries studied constitutes a strong hypothesis. Hence, results obtained here represent a proof of concept, but properly calibrated coefficients should be used for rigorous design.

Fig. 11 shows the results obtained when fixing the superheating at the evaporator exit equal to zero (saturated vapour), while adapting the value of the superheating at the generator exit for each fluid to have saturated vapour at the primary nozzle throat. This choice was made so that that condensation does not affect the choking of the primary fluid. Reaching the state of saturated vapour at the primary nozzle throat means that wet fluids should be superheated at the ejector inlet, isentropic fluids should be saturated while dry fluid should can be in the state of saturated mixture (relying on the validity of the homogeneous equilibrium assumption). **Table 2** details the quality $x_{p,0}$ (if the fluid is a saturated mixture) or superheat $T_{sh,p,0}$ (if the fluid is superheated) of the primary flow leaving the generator, while **Table 3** presents an example of the diameters of the mains sections of the ejectors designed for each fluid studied for three different generator temperatures.

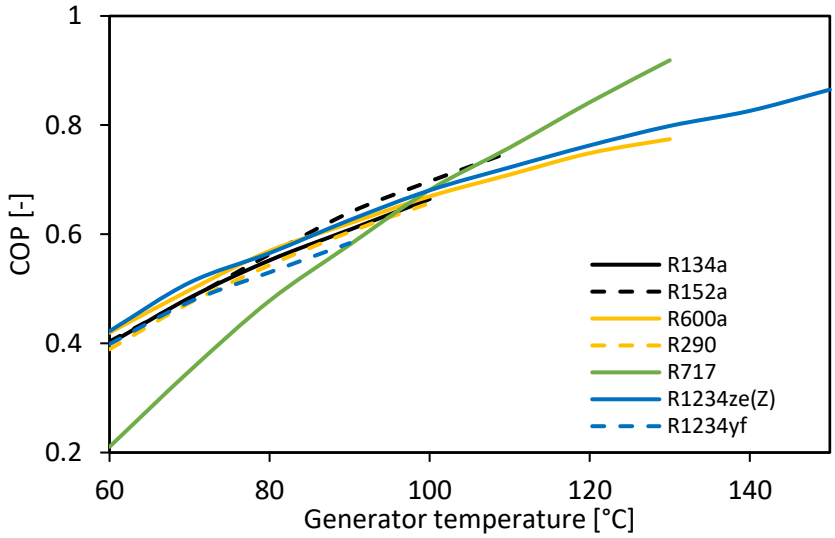

Fig. 11 - COP of the designed SERS cycle for different generator temperatures, for each study fluids. The generator outlet quality/superheat is chosen so to reach a quality of 1 at the primary nozzle throat.

The generator temperature range considered is between 60-150 °C, but the analysis for each fluid is limited to temperatures below the critical temperature, to avoid modelling of a supercritical SERS cycle. In the temperature range of 60-100 °C, all fluids except R717 yield a similar COP (**Fig. 11**). In particular, for the temperature range 60-100 °C, R152a, R600a and R1234ze(Z) seem to be suitable replacements for R134a given their comparable performance. For temperatures higher than 100 °C, R717 appears to be a very promising fluid for SERS cycles yielding significantly better performances than the rest of the fluids.

Table 2 - Quality $x_{p,0}$ (respectively superheating $T_{sh,p,0}$) of the saturated mixture (respectively superheated fluid) leaving the generator for a primary fluid quality of 1 at the primary nozzle throat.

	R134a		R152a		R290		R600a		R717		R1234yf		R1234ze(Z)	
$T_{p,0}$ [°C]	$x_{p,0}$ [-]	$T_{sh,p,0}$ [°C]	$x_{p,0}$ [-]	$T_{sh,0}$ [°C]	$x_{p,0}$ [-]	$T_{sh,p,0}$ [°C]	$x_{p,0}$ [-]	$T_{sh,p,0}$ [°C]	$x_{p,0}$ [-]	$T_{sh,p,0}$ [°C]	$x_{p,0}$ [-]	$T_{sh,p,0}$ [°C]	$x_{p,0}$ [-]	$T_{sh,p,0}$ [°C]
60	-	1.88	-	3.68	-	2.10	0.97	-	-	19.7	0.99	-	0.99	-
70	-	2.37	-	4.47	-	2.65	0.97	-	-	19.8	-	0.11	0.99	-
80	-	3.02	-	4.87	-	3.47	0.97	-	-	19.8	-	1.47	0.99	-
90	-	3.97	-	4.98	-	4.33	0.95	-	-	19.9	-	2.62	0.99	-
100	-	4.75	-	5.40	-	5.27	0.97	-	-	19.9			0.99	-
110			-	6.12			0.98	-	-	19.9			0.99	-
120							-	0.01	-	19.9			-	0.18
130							-	1.76	-	19.9			-	1.19
140													-	2.23
150													-	3.55

Table 3 - Diameter of the main sections of the ejectors designed for three different generator temperatures for each fluid studied

Generator Temperature	Diameter	R134a	R152a	R290	R600a	R717	R1234yf	R1234ze(Z)
60 °C	$d_{p,t}$ [mm]	9.7	9.4	7.7	11.3	6.1	10.2	15.8
	$d_{p,1}$ [mm]	13.1	12.4	9.6	15.3	7.0	13.7	23.4
	$d_{m,2}$ [mm]	20.7	19.5	14.8	25.6	9.1	12.8	38.7
90 °	$d_{p,t}$ [mm]	6.9	6.7	5.7	7.9	4.2	7.3	10.6
	$d_{p,1}$ [mm]	12.2	11.4	8.9	13.9	6.3	12.8	21.2
	$d_{m,2}$ [mm]	22.7	21.8	16.4	27	11.2	23.8	42.2
120 °C	$d_{p,t}$ [mm]	-	-	-	5.8	3.1	-	7.6
	$d_{p,1}$ [mm]	-	-	-	13.2	5.9	-	19.9
	$d_{m,2}$ [mm]	-	-	-	28.2	12.5	-	44.5

4.2.3 Impact of the superheating definition

Several other comparative studies have been performed on SERS cycles (Besagni et al. [4], Cizungu et al. [48], Selvaraju et al. [49], Chen et al. [50], etc.). However, results concerning the optimal fluid choice are very different and often contrasting. Chen et al. [50] highlighted that an often overlooked parameter, the choice of the superheating, has in reality a very strong impact on final results. Superheating of the vapour at the ejector inlet is often chosen arbitrarily and the same value is considered for each fluid. In this way, some fluids are clearly favoured while others are instead penalized.

In order to highlight the bias that can be introduced by the choice of the superheating, a second comparative study was carried out in which zero superheating is considered at the generator exit for all of the seven study fluids. **Fig. 12** shows the results obtained in this case. It appears this time that R152a and especially R717 give better COP when compared to other fluids, even in the 60-100 °C temperature range, in which R717 appeared to give the worst results out of all fluids considered in **Fig. 11**. This is because R152a and R717 are two wet fluids, favoured by the choice of a zero superheating compared to the high superheating needed to prevent condensation before the primary nozzle throat. It is apparent that the choice of a constant superheating is not always suitable for a proper comparison of different fluids and that adapting this parameter to each fluid would be preferable. However, there is still no consensus as to how this choice should be made: for example, it can be defined so as to avoid condensation before the primary nozzle sonic section (see **Fig. 11**), or to avoid any condensation in the ejector, etc. Further experimental studies focusing on the impact of superheating, condensation and flashing within the

ejector are needed to get a better understanding of these phenomena and help in the determination of the correct superheating depending on the fluid characteristics. Note that for the sake of simplicity the superheating level at the evaporator exit was chosen constant (equal to 0°C) for all the studied fluids. However, the same consideration regarding the choice of the superheating apply also in this case and further experimental data is needed for a correct choice.

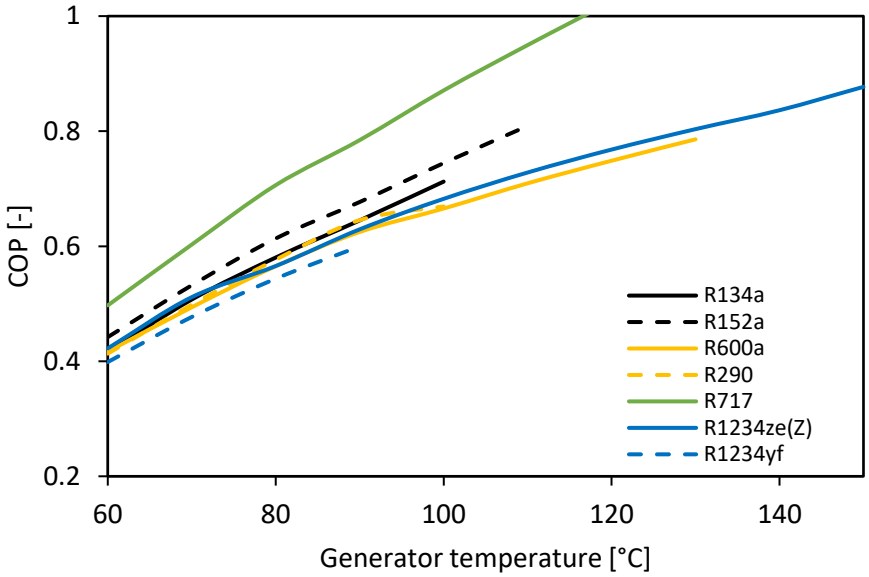

Fig. 12 - COP of the designed SERS cycle for different generator temperatures, for the seven study fluids. The generator outlet superheat is fixed to 0°C for all cases.

4.2.4 Two-phase flow model

As stated in the previous section, results of this model as well as of previous similar thermodynamic models, in case of two-phase flow, rely on the validity of the homogeneous equilibrium assumption. However, the rapid expansion of a one-component mixture through a converging nozzle is not expected to follow a thermodynamic equilibrium path. In normal nozzle configurations, there is little time for mass transfer to take place, and it is reasonable to assume that the amount of mass transferred in the expansion is negligible [51] and that the quality of the vapour in the throat section is equal to the quality at inlet. This is coherent with experimental works carried out on nuclear steam turbines [52] and on ORC supersonic impulse axial micro turbines [53]. Since the vapour entrains liquid droplets, the homogeneous equilibrium assumption leads to lower calculated mass flow rates than experimentally verified.
Different authors suggested the introduction of a modification in the calculation of an injector mass flow rate, including a dependency from two-phase conditions [53][54][55][56]:

$$\dot{m}_{2p} = \frac{\dot{m}_{1p}}{\sqrt{x_0}} \tag{48}$$

In **Eq. (48)**, x_0 is the quality of the fluid entering the ejector, $\dot{m}_{2p}$ is the two-phase mass flow rate and $\dot{m}_{1p}$ is the mass flow rate of a one-phase flow entering the ejector with the same pressure and temperature, but quality equal to one. Recent study carried out at CEA Grenoble on a partial admission axial turbine with a stator made up of a single converging-diverging injector confirm this observation [53][54] for different pure working fluids (Novec649™, HFE7000 and HFE7100) as well as a zeotropic mixture (Novec649™/HFE7000). Therefore, the introduction of **Eq. (48)** was tested in the model.

Fig. 13 shows results of the 1D model assuming homogeneous equilibrium (red curve) and with the introduction of **Eq. (48)** (blue curve) for different primary nozzle vapour inlet quality (primary nozzle inlet temperature and pressure of 100°C and 19.8 bar respectively) in the case of R600a.

The modification proposed increases the mass flow rate treated by the primary nozzle with respect to the hypothesis of homogeneous equilibrium, but reduces the predicted COP of the SERS cycle. Indeed, results of the present 1D model seem to indicate that using a partially evaporated SERS cycle could lead to an increase in the performance of the cycle. On the other hand, the introduction of the correction on treated mass flow rate in the case of two-phase flows shows a decreasing COP when the vapour quality at inlet decreases. It should be highlighted that no additional loss linked to the flashing of the working fluid was considered here, but taking two phase-related irreversibilities into account is necessary for a correct prediction of ejector performance. Further experimental studies are therefore necessary to properly assess the impact of two-phase conditions on treated mass flow rate and ejector performance. Variations of the heat source conditions being frequent in ejector refrigeration cycles, an appropriate modelling of two-phase functioning is important for accurate performance prediction. Finally, a reliable model could be used to evaluate the interest of partially evaporated cycles and to establish if an optimum exists between performance of the cycle and cost of components, due to the smaller size and thermal power necessary in partially evaporated cycles.

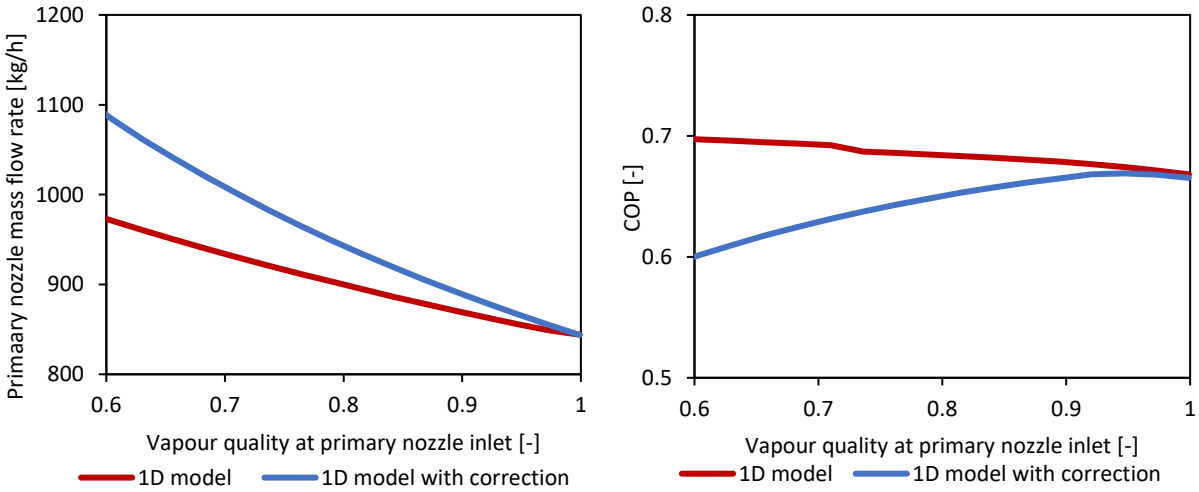

Fig. 13 - Primary mass flow rate and COP of a R600a SERS cycle computed with and without the correction that takes into account two-phase flow impact on the mass flow rate

5 Conclusions

This paper presents a real gas thermodynamic model based on mass flow rate maximization. The model is based on the works of Chen et al. [25], and Metsue et al. [26], but unlike previous models, the procedure proposed simplifies the calculation algorithm and avoids a complex description of the double-choking mechanism at play. Here the novel approach is rather to find both the primary flow and the total ejector mass flow rate by imposing the maximization of mass flow rate. Non-isentropic phenomena are considered through isentropic and mixing efficiencies, which can be used to calibrate the model. Validation in the case of single-phase ejectors was performed with R600a (isobutane) and R134a, and for different ejector geometries, showing that the model is as or more accurate than existing models.

The validated model was used to perform a comparative analysis of the use of different fluids in a SERS cycle for different hot temperature sources. For each operating condition, an optimal ejector geometry was designed. The analysis highlighted that the choice of the superheating, which is often an overlooked parameter, has indeed a strong impact on the cycle performance. The definition of two different criteria for the choice of the superheating in the study lead to different observations with respect to the impact of the refrigerant choice on the performance of the cycle. Since there is still no consensus regarding this choice, further experimental studies are needed to get a better understanding of these phenomena and help in the determination of the correct superheating depending on the fluid characteristics.

Finally, the use of the model in the case of two-phase ejector inlet was tested. Although the model was only validated in the single-phase case, several authors [26] have foreseen the use of such models also for two-phase ejector. Comparison with experimental data on two-phase injectors suggest that correction in the calculated mass flow rate must be included, as well as additional loss terms considering two-phase related irreversibilities. Also, in these cases, additional experimental data is needed to properly assess the impact of the two-phase conditions (such as condensation, flashing, etc.) on ejector performance.

Declaration of Competing Interest

The authors declare that they have no known competing financial interests or personal relationships that could have appeared to influence the work reported in this paper.

Acknowledgements

The authors would like to express their gratitude to the French Alternative Energies and Atomic Energy Commission and the Carnot Energies of the Future Institute. S. Braccio was supported by the CEA NUMERICS program, which has received funding from the European Union Horizon 2020 research and innovation program under the Marie Sklodowska-Curie grant agreement No 800945.

References

[1] S. Braccio, H. Trieu Phan, M. Wirtz, N. Tauveron, N. Le Pierrès, Simulation of an ammonia-water absorption cycle using exchanger effectiveness, Applied Thermal Engineering. (2022) 118712. https://doi.org/10.1016/j.applthermaleng.2022.118712.

[2] A. Godefroy, M. Perier-Muzet, N. Mazet, Thermodynamic analyses on hybrid sorption cycles for low-grade heat storage and cogeneration of power and refrigeration, Applied Energy. 255 (2019) 113751. https://doi.org/10.1016/j.apenergy.2019.113751.

[3] S. Elbel, N. Lawrence, Review of recent developments in advanced ejector technology, International Journal of Refrigeration. 62 (2016) 1–18. https://doi.org/10.1016/j.ijrefrig.2015.10.031.

[4] G. Besagni, R. Mereu, F. Inzoli, Ejector refrigeration: A comprehensive review, Renewable and Sustainable Energy Reviews. 53 (2016) 373–407. https://doi.org/10.1016/j.rser.2015.08.059.

[5] Z. Aidoun, K. Ameur, M. Falsafioon, M. Badache, Current Advances in Ejector Modeling, Experimentation and Applications for Refrigeration and Heat Pumps. Part 1: Single-Phase Ejectors, Inventions. 4 (2019) 15. https://doi.org/10.3390/inventions4010015.

[6] Z. Aidoun, K. Ameur, M. Falsafioon, M. Badache, Current Advances in Ejector Modeling, Experimentation and Applications for Refrigeration and Heat Pumps. Part 2: Two-Phase Ejectors, Inventions. 4 (2019) 16. https://doi.org/10.3390/inventions4010016.

[7] E. Rusly, L. Aye, W.W.S. Charters, A. Ooi, CFD analysis of ejector in a combined ejector cooling system, International Journal of Refrigeration. 28 (2005) 1092–1101. https://doi.org/10.1016/j.ijrefrig.2005.02.005.

[8] K. Pianthong, W. Seehanam, M. Behnia, T. Sriveerakul, S. Aphornratana, Investigation and improvement of ejector refrigeration system using computational fluid dynamics technique, Energy Conversion and Management. 48 (2007) 2556–2564. https://doi.org/10.1016/j.enconman.2007.03.021.

[9] D. Li, E.A. Groll, Transcritical CO2 refrigeration cycle with ejector-expansion device, International Journal of Refrigeration. 28 (2005) 766–773. https://doi.org/10.1016/j.ijrefrig.2004.10.008.

[10] Ø. Wilhelmsen, A. Aasen, K. Banasiak, H. Herlyng, A. Hafner, One-dimensional mathematical modeling of two-phase ejectors: Extension to mixtures and mapping of the local exergy destruction, Applied Thermal Engineering. 217 (2022) 119228. https://doi.org/10.1016/j.applthermaleng.2022.119228.

[11] H. El-Dessouky, H. Ettouney, I. Alatiqi, G. Al-Nuwaibit, Evaluation of steam jet ejectors, Chemical Engineering and Processing: Process Intensification. 41 (2002) 551–561. https://doi.org/10.1016/S0255-2701(01)00176-3.

[12] B. Srinivasan, M. Lad, V. Gaikar, A. Patwardhan, Hydrodynamics and mass transfer characteristics of gas–liquid ejectors, Chemical Engineering Journal. 131 (2007) 83–103. https://doi.org/10.1016/j.cej.2006.12.026.

[13] S. He, Y. Li, R.Z. Wang, Progress of mathematical modeling on ejectors, Renewable and Sustainable Energy Reviews. 13 (2009) 1760–1780. https://doi.org/10.1016/j.rser.2008.09.032.

[14] J.H. Keenan, E.P. Neumann, A Simple Air Ejector, Journal of Applied Mechanics. 9 (1942) 75–82. https://doi.org/10.1115/1.4009187.

[15] J.H. Keenan, E.P. Neumann, F. Lustwerk, An Investigation of Ejector Design by Analysis and Experiment, Journal of Applied Mechanics. 17 (1950) 299–309. https://doi.org/10.1115/1.4010131.

[16] F. Khoury, M. Heyman, W. Resnick, Performance Characteristics of Self-Entrainment Ejectors, Ind. Eng. Chem. Proc. Des. Dev. 6 (1967) 331–340. https://doi.org/10.1021/i260023a013.

[17] S. Aphornratana, S. Chungpaibulpatana, P. Srikhirin, Experimental investigation of an ejector refrigerator: Effect of mixing chamber geometry on system performance, International Journal of Energy Research. 25 (2001) 397–411. https://doi.org/10.1002/er.689.

[18] J. Munday, D. Bagster, A New Ejector Theory Applied to Steam Jet Refrigeration, (1977). https://doi.org/10.1021/I260064A003.
[19] J. Fabri, R. Siestrunck, Supersonic Air Ejectors, in: H.L. Dryden, Th. von Kármán (Eds.), Advances in Applied Mechanics, Elsevier, 1958: pp. 1–34. https://doi.org/10.1016/S0065-2156(08)70016-4.
[20] I.W. Eames, S. Aphornratana, H. Haider, A theoretical and experimental study of a small-scale steam jet refrigerator, International Journal of Refrigeration. 18 (1995) 378–386. https://doi.org/10.1016/0140-7007(95)98160-M.
[21] B.J. Huang, J.M. Chang, C.P. Wang, V.A. Petrenko, A 1-D analysis of ejector performance, International Journal of Refrigeration. 22 (1999) 354–364. https://doi.org/10.1016/S0140-7007(99)00004-3.
[22] I.W. Eames, S. Wu, M. Worall, S. Aphornratana, An experimental investigation of steam ejectors for applications in jet-pump refrigerators powered by low-grade heat, Proceedings of the Institution of Mechanical Engineers, Part A: Journal of Power and Energy. 213 (1999) 351–361. https://doi.org/10.1243/0957650991537734.
[23] Y.-M. Chen, C.-Y. Sun, Experimental study of the performance characteristics of a steam-ejector refrigeration system, Experimental Thermal and Fluid Science. 15 (1997) 384–394. https://doi.org/10.1016/S0894-1777(97)00006-X.
[24] W. Chen, M. Liu, D. Chong, J. Yan, A.B. Little, Y. Bartosiewicz, A 1D model to predict ejector performance at critical and sub-critical operational regimes, International Journal of Refrigeration. 36 (2013) 1750–1761. https://doi.org/10.1016/j.ijrefrig.2013.04.009.
[25] W. Chen, C. Shi, S. Zhang, H. Chen, D. Chong, J. Yan, Theoretical analysis of ejector refrigeration system performance under overall modes, Applied Energy. 185 (2017) 2074–2084. https://doi.org/10.1016/j.apenergy.2016.01.103.
[26] A. Metsue, R. Debroeyer, S. Poncet, Y. Bartosiewicz, An improved thermodynamic model for supersonic real-gas ejectors using the compound-choking theory, Energy. 238 (2022) 121856. https://doi.org/10.1016/j.energy.2021.121856.
[27] A. Bernstein, W.H. Heiser, Compound-compressible nozzle flow, Transactions of the ASME. (1967) 548–554.
[28] O. Lamberts, P. Chatelain, N. Bourgeois, Y. Bartosiewicz, The compound-choking theory as an explanation of the entrainment limitation in supersonic ejectors, Energy. 158 (2018) 524–536. https://doi.org/10.1016/j.energy.2018.06.036.
[29] Choked flow - A generalization of the concept and some experimental data. | AIAA Journal, (n.d.). https://arc.aiaa.org/doi/10.2514/3.3343 (accessed October 27, 2022).
[30] N. Ruangtrakoon, T. Thongtip, S. Aphornratana, T. Sriveerakul, CFD simulation on the effect of primary nozzle geometries for a steam ejector in refrigeration cycle, International Journal of Thermal Sciences. 63 (2013) 133–145. https://doi.org/10.1016/j.ijthermalsci.2012.07.009.
[31] F. Mazzelli, A. Milazzo, Performance analysis of a supersonic ejector cycle working with R245fa, International Journal of Refrigeration. 49 (2015) 79–92. https://doi.org/10.1016/j.ijrefrig.2014.09.020.
[32] S. Croquer, Y. Fang, A. Metsue, Y. Bartosiewicz, S. Poncet, Compound-choking theory for supersonic ejectors working with real gas, Energy. 227 (2021) 120396. https://doi.org/10.1016/j.energy.2021.120396.
[33] Y. Zhu, Y. Li, Novel ejector model for performance evaluation on both dry and wet vapors ejectors, International Journal of Refrigeration. 32 (2009) 21–31. https://doi.org/10.1016/j.ijrefrig.2008.08.003.
[34] Z. Ma, H. Bao, A.P. Roskilly, Thermodynamic modelling and parameter determination of ejector for ejection refrigeration systems, International Journal of Refrigeration. 75 (2017) 117–128. https://doi.org/10.1016/j.ijrefrig.2016.12.005.
[35] F-Chart Software, EES, Engineering Equation Solver, n.d. https://fchartsoftware.com/ees/.
[36] S. Braccio, H.T. Phan, N. Tauveron, N. Le Pierrès, Study of the integration of a supersonic impulse turbine in a NH_3 / H_2O absorption heat pump for combined cooling and power production from a low temperature heat source, E3S Web Conf. 312 (2021) 08018. https://doi.org/10.1051/e3sconf/202131208018.
[37] Simone Braccio, Antonio Di Nardo, Giorgio Calchetti, Hai Trieu Phan, Nolwenn Le Pierrès, Nicolas Tauveron, Performance evaluation of a micro partial admission impulse axial turbine in a combined ammonia-water cooling and electricity absorption cycle, Sumbitted May 2022. (n.d.).
[38] H. Saravanamuttoo, G. Rogers, H. Cohen, P. Straznicky, Gas Turbine Theory, 6th ed., Pearson Prentice Hall, Harlow, England; New York, 2009.
[39] M. Khennich, N. Galanis, M. Sorin, Effects of design conditions and irreversibilities on the dimensions of ejectors in refrigeration systems, Applied Energy. 179 (2016) 1020–1031. https://doi.org/10.1016/j.apenergy.2016.07.053.
[40] F. Liu, E.A. Groll, Study of ejector efficiencies in refrigeration cycles, Applied Thermal Engineering. 52 (2013) 360–370. https://doi.org/10.1016/j.applthermaleng.2012.12.001.

[41] J. Liu, L. Wang, L. Jia, X. Wang, Thermodynamic model for all modes performance analysis of supersonic ejector considering non-uniform distribution of flow field, International Journal of Refrigeration. 96 (2018) 17–24. https://doi.org/10.1016/j.ijrefrig.2018.08.023.
[42] S. Braccio, H.T. Phan, N. Tauveron, N. Le Pierrès, Study of a cold and electric cogeneration machine using a low temperature heat source., (2021). https://doi.org/10.25855/SFT2021-036.
[43] D. Butrymowicz, K. Śmierciew, J. Karwacki, J. Gagan, Experimental investigations of low-temperature driven ejection refrigeration cycle operating with isobutane, International Journal of Refrigeration. 39 (2014) 196–209. https://doi.org/10.1016/j.ijrefrig.2013.10.008.
[44] A. Hakkaki-Fard, Z. Aidoun, M. Ouzzane, A computational methodology for ejector design and performance maximisation, Energy Conversion and Management. 105 (2015) 1291–1302. https://doi.org/10.1016/j.enconman.2015.08.070.
[45] G. Besagni, F. Inzoli, The influence of Variable Geometry Control on a R290 Ejector Refrigeration System, J. Phys.: Conf. Ser. 2177 (2022) 012010. https://doi.org/10.1088/1742-6596/2177/1/012010.
[46] G. Besagni, N. Cristiani, L. Croci, G.R. Guédon, F. Inzoli, Multi-scale evaluation of ejector performances: The influence of refrigerants and ejector design, Applied Thermal Engineering. 186 (2021) 116502. https://doi.org/10.1016/j.applthermaleng.2020.116502.
[47] R. Ciconkov, Refrigerants: There is still no vision for sustainable solutions, International Journal of Refrigeration. 86 (2018) 441–448. https://doi.org/10.1016/j.ijrefrig.2017.12.006.
[48] K. Cizungu, A. Mani, M. Groll, Performance comparison of vapour jet refrigeration system with environment friendly working fluids, Applied Thermal Engineering. 21 (2001) 585–598. https://doi.org/10.1016/S1359-4311(00)00070-3.
[49] A. Selvaraju, A. Mani, Analysis of an ejector with environment friendly refrigerants, Applied Thermal Engineering. 24 (2004) 827–838. https://doi.org/10.1016/j.applthermaleng.2003.08.016.
[50] J. Chen, H. Havtun, B. Palm, Screening of working fluids for the ejector refrigeration system, International Journal of Refrigeration. 47 (2014) 1–14. https://doi.org/10.1016/j.ijrefrig.2014.07.016.
[51] R.E. Henry, H.K. Fauske, The Two-Phase Critical Flow of One-Component Mixtures in Nozzles, Orifices, and Short Tubes, Journal of Heat Transfer. 93 (1971) 179–187. https://doi.org/10.1115/1.3449782.
[52] A. Leyzerovich, Wet-steam Turbines for Nuclear Power Plants, PennWell Books Ed., 2005.
[53] G. Lhermet, N. Tauveron, N. Caney, Q. Blondel, F. Morin, A Recent Advance on Partial Evaporating Organic Rankine Cycle: Experimental Results on an Axial Turbine, Energies. 15 (2022) 7559. https://doi.org/10.3390/en15207559.
[54] N.Tauveron, G. Lhermet, N. Caney, Experimental results of a partially evaporated organic Rankine cycle including a two-phase axial turbine., in: HEFAT 2022, 2022.
[55] C. Herer, Elements of thermal hydraulics and applications to nuclear reactors, (2017). https://doi.org/10.13140/RG.2.2.12982.50243.
[56] J.C. Leung, Easily size relief devices and piping for two-phase flow, Chemical Engineering Progress. 92 (1996). https://www.osti.gov/biblio/419821.